Spacecraft Charging Model

G.T. Inouye*
TRW Systems, Redondo Beach, Calif.

An electrical equivalent circuit model of a specific spacecraft configuration is developed. The response of this model to a geomagnetic substorm is obtained by representing the environmental parameters by equivalent current generators, which then constitute the forcing functions. The results show that the seasonal and diurnal variation of differential charging potentials are consistent with the observed occurrence of anomalous events on operational spacecraft. The model also shows how stresses may be reduced by incorporating relatively minor modifications to the spacecraft configuration. The effects of uncertainty in the available environmental and materials parameters are discussed.

Introduction

An increasing body of evidence exists for the correlation between the occurrence of anomalous behavior of satellites in geosynchronous orbit and unusual environmental perturbations observed by both ground-based and spacecraft diagnostics. DeForest[1,2] first published evidence from ATS-5 of spacecraft charging to potentials as high as −9 kv in earth eclipse. He showed how this phenomenon was related to the injection of energetic electrons during geomagnetic substorm activity into the local morning sector of the magnetosophere at synchronous orbit altitudes. The correlation of the observed anomalous events with ground-based magnetograms or even with other synchronous orbit satellite diagnostics on a one-for-one basis is generally poor. This lack of correlation is at least partially explained in this paper in terms of the time required for the buildup and decay of potential differences for the specific spacecraft geometric configuration and orientation relative to solar ultraviolet radiation.

Once the possibility of spacecraft charging, and more specifically, differential charging of different parts of a given spacecraft to multikilovolt levels is accepted, arc discharges may be postulated as being the mechanism whereby electrical circuits are caused to misbehave or even be damaged permanently. The properties of these arc discharges and the transfer functions whereby they couple into specific electrical circuits are subjects of current investigations and will not be discussed here. Shaw[3] and Cauffman and Shaw[4] discuss the most direct evidence available of the existence of arc discharges on a synchronous orbit spacecraft.

Many studies have been performed of the behavior of spacecraft in the substorm environment.[5-8] Of related work, papers by Knott[9] and Knott, Grard, and Pedersen[10] are examples of studies of photoemission and secondary emission as they affect the potentials of a homogeneous spherical spacecraft in a hot plasma environment. The present paper, an extension of prior work, represents a first-order model of a real spacecraft. The results of calculations with this model are consistent with the observed seasonal variations of the occurrence of anomalous events on two slightly dissimilar pairs of a generic communications spacecraft series which were launched in 1971 (Flight 1 and 2) and 1973 (Flights 3 and 4). Orbital experience with respect to both satellite pairs provided the basis for the development of the spacecraft charging model. As a result of the model calculations, a set of modifications has been incorporated into the follow-on spacecraft of this series (Flights 5 and 6).

Presented as Paper 75-255 at the AIAA 13th Aerospace Sciences Meeting, Pasadena, California, January 20-22, 1975; submitted February 7, 1975; revision received June 13, 1975. The work presented here was funded under Air Force Contract FO 4701-69-C-0091. I would like to acknowledge the guidance from A. Rosen, the data provided by J.M. Sellen and S.E. DeForest, the analysis of the ATS-5 data performed by J.O. Vogl, and the contributions of J.W. Capps of the Aerospace Corp. in reviewing the model calculations at various stages of development and in suggesting refinements and corrections that effected the final results. The numerical computations were undertaken with the support of J.L. Wilson. In addition, the support of J. Durschinger and the 777 Project Office is greatly appreciated.

Index category: Spacecraft Configurational and Structural Design (including Loads).

*Senior Staff Scientist.

Background

The occurrence of anomalous events on Flights 1 and 2 were noted almost immediately after launch. These events, it turned out, were of a special type, which we shall designate as "R." In Refs. 5 and 11 an extremely good correlation was established between these events and geomagnetic activity as recorded on ground-based magnetograms. The predominant occurrence of events in the midnight-dawn sector also conformed to expectations from magnetospheric theory. The circuitry associated with the "R" type of anomalies was shut off in late 1971 on Flights 1 and 2. The circuits were modified for Flights 3 and 4, and "R" type anomalies have been eliminated on these spacecraft. Subsequently, however, another class of anomalies ("T") was observed. Although the total number for the two spacecraft[13], (including failures) over the period of two years was small, the statistic seemed to indicate a preference for events occurring during the equinox seasons.

Figure 1 shows the timing of events on Flight 3 and 4 from launch in Dec. 1973 through mid-November 1974. At the top of Fig. 1, events of each type for each spacecraft are shown as a function of local time. The daily geomagnetic activity indices are recorded at Fredricksburg and Anchorage are shown in the lower portion. The A-indices for these two stations, which are widely separated in longitude and latitude, show a gross, but not detailed, correlation with each other. The Anchorage station, which is located in the auroral belt, is expected to provide data relative to substorm activity. It longitude, however, is 35° away from the nearest of the two spacecraft, and it also differs by 9° in geomagnetic latitude from that of the footprint on the ground of the field line passing through that spacecraft. The correlation of ground-based diagnostics with substorm phenomena at synchronous orbit altitudes is extremely difficult because of the localized nature of the effects and the unavailability of a network of properly located observational stations. Note in Fig. 1 that two additional classes of events ("C" and "S") have been observed on Flight 4. Flight 3 has had no events since April 10, 1974, and all of the remainder have occurred on Flight 4.

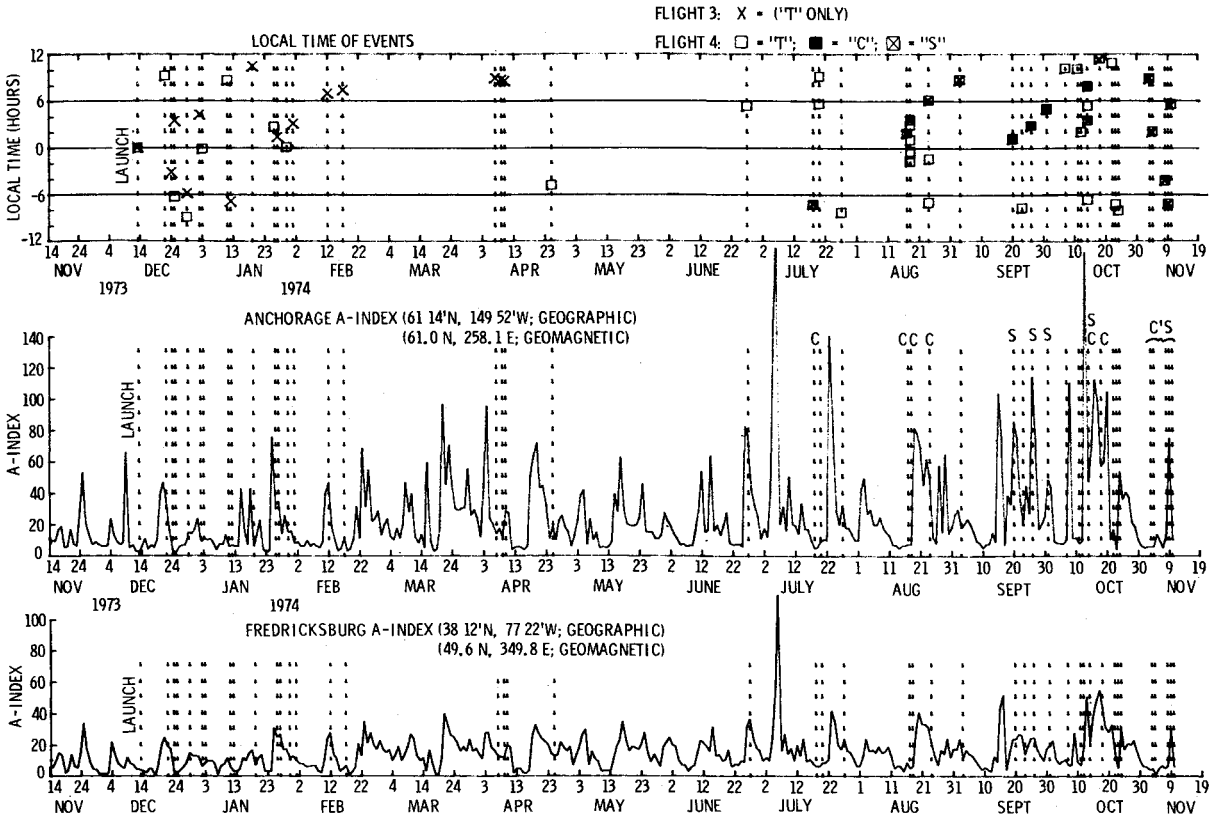

Fig. 1 Timing of events on Flights 3 and 4 and the daily A-Indices from Fredricksburg and Anchorage.

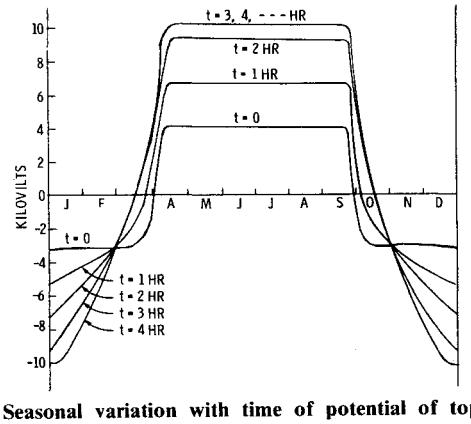

Fig. 2 Seasonal variation with time of potential of top surface relative to spacecraft ground.

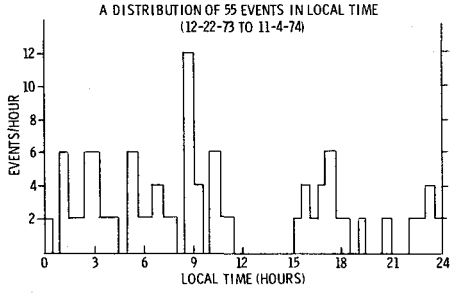

Fig. 3 Distribution of 55 events in local time (12-22-73 to 11-4-74).

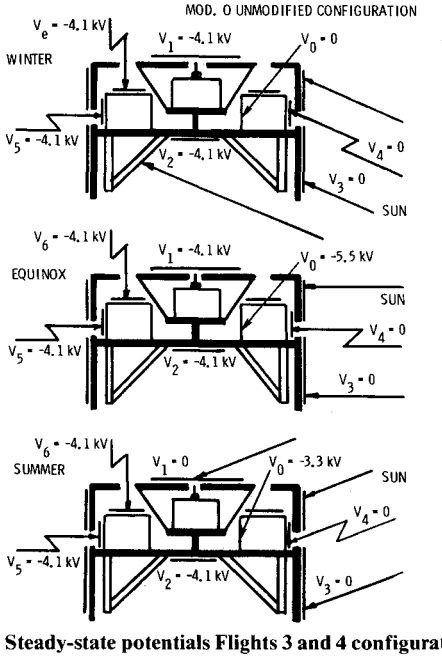

Fig. 4 Steady-state potentials Flights 3 and 4 configurations.

There is no explanation for this difference in behavior. It should be noted, however, that they are located approximately 180° apart in longitude and 11° (+6° and −5°) in geomagnetic latitude. Except for the "S" events, the correlation of the totality of events with the A-Indices is not particularly evident. On selected events such as the Flight 2 failure on June 2, 1973, however, an extremely good correlation with an unusually violent environmental disturbance has been established.[6]

Figure 1 shows a clear absence of events for a 49-day period surrounding the spring equinox. However, the failure of a pressure transducer during this period is not shown. During the fall equinox, a period of 41 days may be noted in which "C"-type anomalies are absent. Except for one "T" event on Sept. 23, a 44-day absence period also exists for these events. The four "S" events, in contrast, occurred during the fall equinox.

Figure 2 shows the seasonal variation of the stress, or the potential difference between the forward closure dielectric surfaces and spacecraft ground, as developed in the zeroth-

order spacecraft charging model. The model was developed in mid-March of 1974, when the absence of "T"-type anomalies became evident in spite of increased geomagnetic activity as compared to the two previous months. The refinements of the first-order model presented here do not change the essential results of the zeroth order and its predictions of future anomalous events.

Figure 3 shows the distribution in local time of 55 events on Flights 3 and 4. The predominance of events in the midnight-morning hours is an indication that statistically, at least, these events may be related to the environment. The evening and morning peaks, which are evident in Fig. 3, may be a manifestation of the diurnal peaking of exposed metallic surface, as will be discussed in this paper. Finally, it should be reported that a considerable effort was expended in searching for internal and other external sources for each of these anomalous events. Internal sources investigated related to possible spontaneous degradation of critical components. External sources included interference from ground-based sources and from other in-orbit satellites. In all cases it was concluded that these alternative sources were even more unlikely candidates than the synchronous orbit environment itself.

Spacecraft Configuration

Figure 4 shows schematic representations of the generic spacecraft configuration, with its orientation relative to sunlight during the three seasons. Four solar array panels constitute the cylindrical main body, which is attached to the central spinning platform. Electronic boxes related to the "R" and "S"-type anomalies are located on this spinning platform, as is the pressure transducer. These subsystems are exposed to the environment by four portholes in the solar array, and by narrow slits between solar array panels. The upper central section constitutes the despun portion of the spacecraft on which the earth-pointing antennas are located. Equipment in which the "T" and "C"-type events occurred are located on the despun platform. Although there is no access for either sunlight or plasma into the despun section, tests with arc discharge sources have shown that discharges in the forward closure area can cause "T"-type anomalies. A narrow annular gap in the forward closure between spinning and despun sections also permits plasma and some sunlight (during summer months) to enter into the region of the spinning platform equipment.

A notable and important feature of the spacecraft is that less than 5% (1.0 m^2 out of 24 m^2), of the total exterior surface is metallic and tied to spacecraft ground. Figure 5 shows the seasonal and diurnal variation of the metallic surface area which is exposed to sunlight. The major portion of this exposed metal consists of 1- and 2-in. diameter aluminum structural pipes located in the lower portion of the spacecraft. These pipes are depicted as triangular structures inside the lower half of the spacecraft drawings shown in Fig. 4. Since the lower portion is spinning rapidly, the areas exposed to sunlight are averaged over the spin period. The diurnal variation shown in the lower portion of Fig. 5 is due entirely to waveguides, which feed the earth-pointing dish antennas. Nearly all exterior surfaces are covered or wrapped with thermal blankets, second surface mirrors, or, in the case of the solar array, with solar cell cover glasses. Subsequent examination of a number of other spacecraft configurations has shown that the small proportion of exposed metallic surface relative to dielectric surface areas (thermal blankets, solar cell cover glass, second surface mirrors, paints, etc.) is a common feature which has been primarily dictated by thermal control considerations. One of the important results of the study reported here is to emphasize the importance of considering the selection of materials for spacecraft charging as well as for thermal, structural, and other properties.

Various steady-state potentials with respect to the plasma at infinity resulting from the application of a step-function sub-

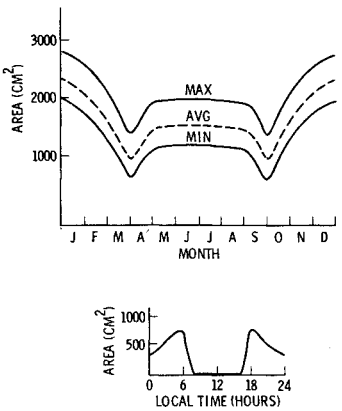

Fig. 5 Seasonal and dirunal variation of exposed metallic areas for photoemission. The diurnal variation applies to all seasons.

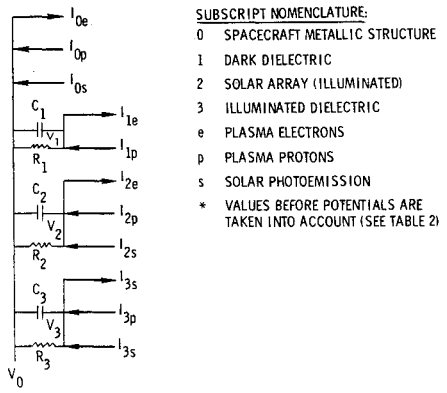

Fig. 6 Spacecraft charging model.

storm are also shown in Fig. 4. These potentials are introduced here to emphasize the fact that different dielectric surfaces do attain different potentials relative to spacecraft ground. The potential and capacitance (and leakage) to spacecraft ground of each surface affects the potential of spacecraft ground as well as the potential of every other surface.

Description of Spacecraft Charging Model

The charging model shown in Fig. 6 is an electric circuit representation of a specific spacecraft configuration. The basic metallic surface and all of the metallic objects tied to it constitute the reference mode for the circuit. Its potential, spacecraft "ground," is designated as V_0. Various dielectric and ungrounded metallic surfaces exposed to the ambient plasma are represented as "leaky" capacitors. Each dielectric surface which is expected to charge uniformly as an equipotential surface is shown as a separate capacitor. One end of each capicitor is tied to the reference (V_0) node. The other end of each capicitor as well as the V_0 node itself constitute nodes to which current generators are connected representing the charging and discharging sources; i.e., plasma electrons and protons, photo-emission, and secondary emission. The return node for all of these current generators is the zero potential reference at infinity.

In general, the magnitudes of the circuit component values, capacitance and leakage conductance are proportional to the areas involved. Table 1 lists the typical per unit area parameters assumed for each material. Figure 7 shows a preliminary set of experimental data points obtained for 2-mil Kapton thermal blanket material, which indicate that the effective bulk conductivity of Kapton, 10^{-18} (Ω-cm), exhibits a threshold electrostatic stress of about 240 kv/cm.[12] Above this threshold, the conductivity increases as the 3.5th power of stress (current as the 4.5th power of stress).

Table 1 Material parameters and per unit area capacitances and resistances

ITEM	DI-ELECTRIC CONSTANT	RESIS-TIVITY (OHM-CM)	τ (SECONDS)	THICK-NESS (MILS)	CAPACITANCE PER CM^2 (PF)	RESISTANCE PER CM^2 (OHMS)
*2 MIL KAPTON OR MYLAR THERMAL BLANKET	3	10^{18}	$2.65 \cdot 10^5$	2	52.2	$5.08 \cdot 10^{15}$
*1/2 MIL THERMAL BLANKET	3	10^{18}	$2.65 \cdot 10^5$	.5	208.9	$1.27 \cdot 10^{15}$
**SOLAR CELL COVER GLASS	3	10^{19}	$2.65 \cdot 10^6$	6	17.41	$1.524 \cdot 10^{17}$
*SECOND SURFACE MIRRORS	3	10^{19}	$2.65 \cdot 10^6$	8	13.05	$2.04 \cdot 10^{17}$
RTV ON S.S. MIRRORS	3	10^{18}	$2.65 \cdot 10^5$	.35	298.4	$8.94 \cdot 10^{15}$
FIBERGLASS ON ALUMINUM HONEYCOMB	3	10^{18}	$2.65 \cdot 10^5$	10	2.06	$1.288 \cdot 10^{17}$
PAINT	2	10^{15}	$1.77 \cdot 10^2$	3	23.21	$7.62 \cdot 10^{12}$

*$R = K_1 V^{-3.5}$ FOR V > 1.2 KV **$R = K_2 V^{-3.5}$ FOR V > 4.8 KV

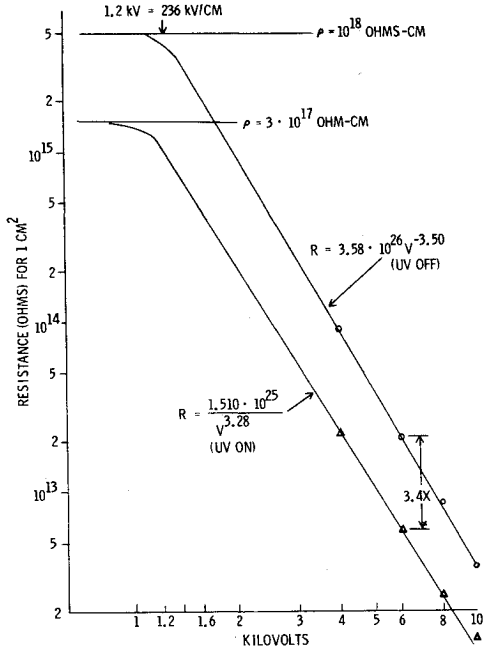

Fig. 7 Voltage and UV sensitivity of 2 mil Kapton resistance (data from M.J. Sellen).

In an examination of the particular spacecraft discussed here, 18 different capacitors (dielectric surface areas) were identified. Only four of these were used in the circuit analysis, since they represented the majority of the total area, and would control the reference node potential V_0. Potentials of surfaces not included in the basic analysis were calculated with the assumption that V_0 is not affected by these smaller contributors. Aperature/cavity potentials, for instance, were calculated in this way.

Only three capacitors are shown in the equivalent circuit of Fig. 6 because two of them were combined to form C_1 which represents all dielectric surfaces which are not illuminated by solar photons. C_2 represents the illuminated solar cell array cover glass (quartz). A smaller parallel and also illuminated capicitor, C_3 (Kapton), was included in order to permit introduction of a nonlinear element from the reference node to the zero potential node at infinity. The value of these capacitors, C_1, C_2, C_3, were 4.5 μf, 2.4 μf, and 0.30 μf, respectively, for both winter and equinox seasons. During the summer season a part of the "dark" capacitance, C_1, becomes illuminated and the values of C_1, C_2, C_3 become 3.0 μf, 2.0 μf, and 1.8 μf, respectively. The leakage resistances were adjusted to correspond to the appropriate dielectric surface areas. In a more generalized analysis where many more capacitive elements are to be included, a more systematic procedure should be used in which the seasonal and diurnal variations are incorporated only into the definitions of the current sources.

Current Sources for Model

The various charging and discharging mechanisms constitute the forcing functions for the spacecraft charging model. In every case, electron and proton charging, photoemission, and secondary emission, the source is not representable as a simple linear function of potential. Because of the nonlinear nature of these current sources, as well as of the bulk conductivity, the analysis was carried out with a computer. Table 2 lists the functional equations which relate currents to potentials. Also listed in Table 2 are the assumed parameters which define the substorm plasma, and the photoemission and secondary emission characteristics for dielectrics and metals.

The factor $f = 2(m_e T_p / m_p T_e)^{1/2} = 0.066$ converts electron currents to proton currents via the requirement for charge neutrality in the plasma. It includes an additional factor of 2 to account for the fact that secondaries are assumed to be negligible for incident protons, but account for one-half of the incident electrons, in the case of metals. For dielectric surfaces, only a fourth of the incident electrons are assumed to "stick," and this accounts for the $2f$ factor used for calculating proton currents I_{1p}, I_{2p}, and I_{3p}.

Figure 8 shows a typical geomagnetic substorm variation of the four parameters, electron and proton temperatures, and currents, as a function of time. The data for this figure were taken from the ATS-5 plasma experiment. This description of the substorm as well as the functional form of the current source assumes a Maxwell-Boltzmann energy distribution which DeForest[2] states is a fair approximation. Recent information from S.E. DeForest on his ATS-6 experiment, indicating an occasional strongly field-aligned component of particle flux, has not been considered in this analysis. Table 3 summarizes the ATS-5 data obtained over a 3-month period in 1970. It should be noted that the ATS-5 plasma experiment does not detect electrons with energies below 50 ev. From proton data taken during eclipse when the spacecraft is charged, DeForest infers that the thermal electron density is small compared to the energetic electron density. This deficiency may be noted in the quiet time parameters presen-

Table 2 Assumed parameters and voltage dependence equations for the current generators

EQUATIONS FOR CURRENTS	ASSUMED PARAMETERS
$I_{0e} = I_{0e}^* (1 - \frac{V_0}{T_e}) e^{V_0/T_e}$	$J_e = 1.5$ NA/CM^2
$I_{0p} = f\, I_{0e}^* e^{-V_0/T_p}$	$J_{\text{secondaries metals}} = 0.5\, J_e$
$I_{0s} = I_{0s}^* e^{-V_0/2}$ VOLTS $(V_0 > 0)$	$J_{\text{secondaries dielectrics}} = 0.75\, J_e$
$I_{1e} = I_{1e}^* e^{V_1/T_e}$	$J_p = .033\, J_e$
$I_{1p} = 2f\, I_{1e}^* e^{-V_1/T_p}$	where $.033 = \left[\frac{m_e}{m_p} \cdot \frac{T_p}{T_e}\right]^{1/2}$
$I_{1s} = I_{1s}^* e^{-V_0/2}$ VOLTS ; $(I_{1s}^* = 0)$	$f = 2 \times .033 = .066$
$I_{2e} = I_{2e}^* e^{V_2/T_e}$	$T_p = 2\, T_e$
$I_{2p} = 2f\, I_{2e}^* e^{-V_2/T_p}$	$J_{\text{photo metals}} = 3$ NA/CM^2
$I_{2s} = I_{2s}^* e^{-V_2/2}$ VOLTS $(V_2 > 0)$	$J_{\text{photo dielectrics}} = 1.5$ NA/CM^2
$I_{3e} = I_{3e}^* e^{V_3/T_e}$	$T_p = 2\, T_e$
$I_{3p} = 2f\, I_{3e}^* e^{-V_3/T_p}$	
$I_{3s} = I_{3s}^* e^{-V_3/2}$ VOLTS $(V_3 > 0)$	

*SUBSCRIPT NOMENCLATURE GIVEN IN FIGURE 6.

ted in Table 3, which would clearly indicate a lack of electrons for charge neutrality.

$$\frac{J_e}{J_p} \cong \frac{35 \text{ pa}}{2.5 \text{ pa}} = 14$$

$$\left[\frac{m_p T_e}{m_e T_p}\right]^{1/2} \cong \left[1840 \cdot \frac{3.5 \text{ kev}}{14 \text{ kev}}\right]^{1/2} = 21.5$$

The substorm data for Fig. 8, on the other hand, do nearly satisfy the chrage neutrality test.

$$\frac{J_e}{J_p} \cong \frac{600 \text{ pa}}{20 \text{ pa}} = 30$$

$$\left[\frac{m_p T_e}{m_e T_p}\right]^{1/2} \cong \left[1840 \cdot \frac{10 \text{ kev}}{18 \text{ kev}}\right]^{1/2} = 31.2$$

For the purposes of the present analysis, a step-function substorm current density of 1.5 na/cm^2 at time $t = 0$ was assumed with the electron temperatures varying from 1.5 to 10 kev. The proton temperature was assumed to be twice that of the electrons, and the ratio of proton to electron flux was adjusted for the mass and temperature ratios. Secondary emission currents were assumed to be 50% of the incident electron current for metallic and 75% for dielectric surfaces. Photoemission current densities of 3 *na*/cm^2 from metals and 1.5 *na*/cm^2 from dielectrics were assumed. These values are in the order of those deduced by DeForest[1] from his analysis of ATS-5 charging data. The larger photoemission from metals as compared to dielectrics, and the larger secondary emission from dielectrics as compared to metals are consistent with laboratory data.

As with the circuit capacitance and resistance magnitudes, the current source magnitudes are also proportional to the appropriate spacecraft areas. Two additional factors were included, however. For photoemission, the areas used are at normal incidence; i.e., planar projections perpendicular to the sun-line. For plasma currents, a field-of-view correction was applied to those areas whose view angles were restricted to less than 2π sterad. Electron charging currents at zero potential ranged from 1 to 50 μa, and photoemission currents from 3 to 60 μa, for different surface areas on the spacecraft.

Results

With the spacecraft charging potentials presented here it was possible to show the existence of voltage stresses which were consistent with the occurrence of arc discharges and the resulting anomalous events in the correct locations and during appropriate seasons of the year. The stresses calculated with the zeroth order model turned out to be true predictions for those anomalies which have occurred since the spring equinox of 1974. The calculations also indicated how relatively minor modifications of the exterior configuration could decrease stresses dramatically. Figure 9 shows schematically the modifications that were incorporated and the calculated steady-state potentials for the new configuration. Specifically, the bare metal pipes in the lower portion of the spacecraft were wrapped with thermal blanket materials to reduce photoemission during the winter months. An equivalent metallic area was emplaced on the forward closure in order to replace the surface area for plasma charging lost by wrapping the pipes. In this location the replacement metal area is not illuminated during the winter and equinox seasons, and serves only to collect plasma currents. The net effect, then, is to approximate the conditions obtained on Flights 3 and 4 during the equinox seasons in which solar illumination of metallic surfaces is a minimum, and the spacecraft "ground" charges to highly negative potentials during geomagnetic substorms. The differential potential between spacecraft ground and the forward closure dielectric surface is minimal, however, and this result is consistent with the absence of "T" and "C" type of anomalies on Flights 3 and 4 during the equinoxes. (see Fig. 1.).

During the summer months the forward closure is illuminated by the sun and the dielectric surface area is clamped to nearly zero potentials by photoemission. In the Flights 3 and 4 configuration, the structure potential is charged to highly negative potentials during substorms because the exposed metallic surface area is small and therefore a high stress condition exists in the forward closure. The location of the grounded replacement metal area on the forward closure in the modified Flights 5 and 6 configuration now clamps the structure to near zero instead of highly negative potentials. Thus, summer stresses are relieved in the forward closure area.

The countermeasures against the equinox "S"-type anomalies on Flights 3 and 4 were based on the fact that these events were associated with equipment located on the spinning platform. Differential potentials in this "cavity" location can only be caused by plasma or sunlight entering via apertures in the solar array panels or the annular gap between the spinning and despun sections in the forward closure. It was also

Table 3 ATS-5 measurements

PLOT OF 2 JAN 1970 SUBSTORM

ELECTRONS

- CURRENTS UP TO 0.85 na/cm^2 FOR ≈ 30 MINUTES
- AVERAGE CURRENT 0.5 na/cm^2 FOR > 8 HOURS
- PEAK TEMPERATURES OF 12-13 KILOVOLTS FOR ≈ 45 MIN
- AVERAGE TEMPERATURE OF ~ 6 KILOVOLTS FOR ≈ 8 HOURS

PROTONS

- CURRENTS UP TO 13 pa/cm^2
- AVERAGE CURRENT 7 pa/cm^2
- PEAK TEMPERATURES OF 16-20 KILOVOLTS FOR ≈ 30 MIN
- AVERAGE TEMPERATURE OF ~ 12 KILOVOLTS

OTHER SUBSTORMS

ELECTRONS

- CURRENTS OBSERVED UP TO 2 na/cm^2, TYPICAL 0.1 TO 0.2
- POSSIBLE: 8 na/cm^2 MAXIMUM (NOISY DATA) FOR 5-10 MIN
- TEMPERATURES UP TO 20-30 KEV
- TYPICAL TEMPERATURE 2-6 KEV

QUIET TIME (e.g., 6-7 FEB 1970)

- ELECTRON CURRENTS OF 20 TO 50 pa/cm^2
- ELECTRON TEMPERATURES OF 2 TO 5 keV
- PROTON CURRENTS OF 2 TO 3 pa/cm^2
- PROTON TEMPERATURES OF 12 TO 16 keV

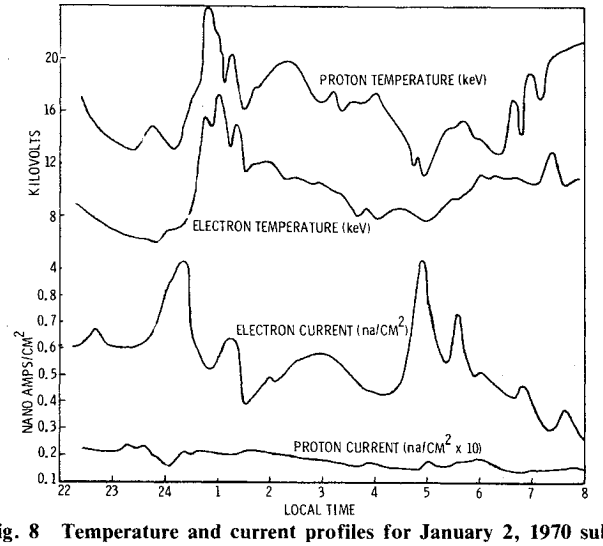

Fig. 8 Temperature and current profiles for January 2, 1970 substorm.

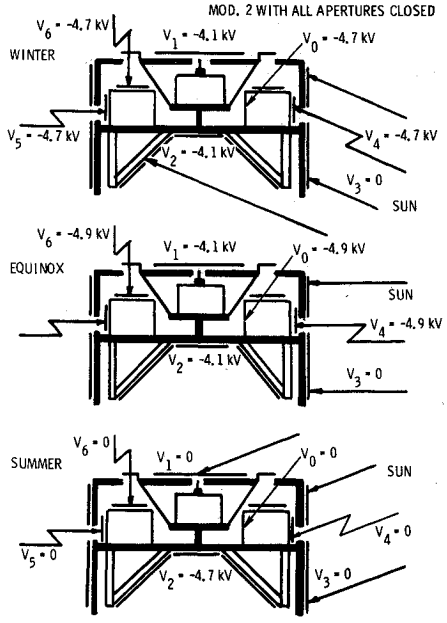

Fig. 9 Steady-state potentials Flights 5 and 6 configuration.

Table 4 Potential differences (kv) at external surfaces

POTENTIAL DIFFERENCES (KV) AT EXTERNAL SURFACES

MOD	WINTER			EQUINOX			SUMMER		
	V_1-V_0	V_2-V_0	V_3-V_0	V_1-V_0	V_2-V_0	V_3-V_0	V_1-V_0	V_2-V_0	V_3-V_0
0	-4.1	-4.1	0	1.4	1.4	-5.5	3.3	-0.8	3.3
1	-2.4	-2.4	1.7	-1.4	-1.4	2.7	0	-4.1	0
2	0.6	0.6	4.7	0.8	0.8	4.9	0	-4.1	0

POTENTIAL DIFFERENCES (KV) AT APERTURES

MOD.	APERTURES CLOSED	WINTER			EQUINOX			SUMMER		
		V_4-V_0	V_5-V_0	V_6-V_0	V_4-V_0	V_5-V_0	V_6-V_0	V_4-V_0	V_5-V_0	V_6-V_0
0	NONE	0	-4.1	-4.1	5.5	1.4	1.4	3.3	-0.8	-0.8
M2	6	4.7	0.6	0	4.9	0.8	0	0	-4.1	0
	4,6	0	0.6	0	0	0.8	0	0	-4.1	0
	4,5,6	0	0	0	0	0	0	0	0	0

MOD. 0 = ORIGINAL CONFIGURATION
MOD. 1 = PIPES WRAPPED ONLY (5462 CM^2)
MOD. 2 = PIPES WRAPPED (5462 CM^2), METAL EXPOSED (3406 CM^2)
SURFACE 0 = METALIC STRUCTURE (SPACECRAFT GROUND)
SURFACE 1 = FORWARD CLOSURE
SURFACE 2 = BOTTOM OF SPINNING PLATFORM
SURFACE 3 = SOLAR CELL COVER GLASS
APERTURE 4 = PORTHOLES AND SLIT ON SOLAR PANELS FOR SUNLIGHT
APERTURE 5 = PORTHOLES AND SLIT ON SOLAR PANELS FOR PLASMA
APERTURE 6 = ANNULAR GAP ON FORWARD CLOSURE FOR PLASMA
V_n = POTENTIAL OF SURFACE n WHERE n = 0, 1, 2, 3, 4, 5, 6

recognized that even small "aperture/cavity" arc discharges are potentially harmful because they could occur very close to susceptible cables and connectors to electronic hardware. The equinox season is when the "S" type events are most likely to occur because the structure charges to the most highly negative potentials, and solar illumination via apertures may create a localized high-stress condition. The reversed polarity situation is also possible in which the structure potential is nearly zero. Plasma entry via apertures in this case causes a high stress by charging a localized dielectric area to a highly negative potential. Closing of all of the apertures in the Flights 5 and 6 configuration eliminates the entrance of high-energy plasma and sunlight in to the cavity.

Table 4 summarizes and shows the reductions in the steady-state potential differences for the original configurations of Fig. 9. Mod 1 is an intermediate configuration in which the metal on the forward closure was not provided to replace that covered by wrapping the pipes. The potentials in Figs. 4 and 9 and in Table 4 apply to the 3 kev electron temperature case with the nonlinear i-v effects excluded.

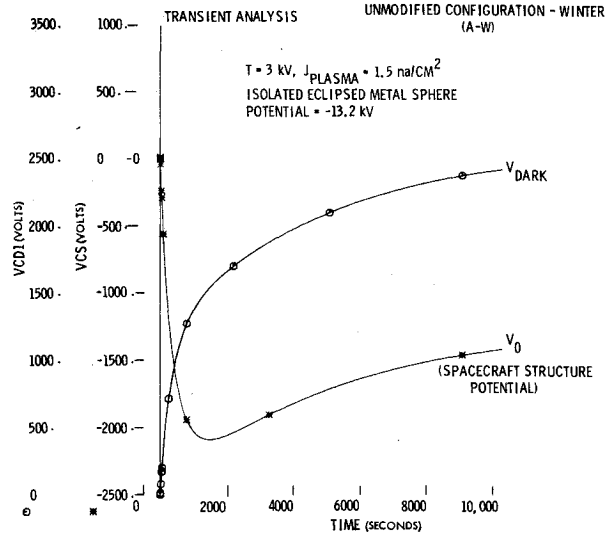

Fig. 10 Transient analysis Flights 3 and 4 configuration (winter).

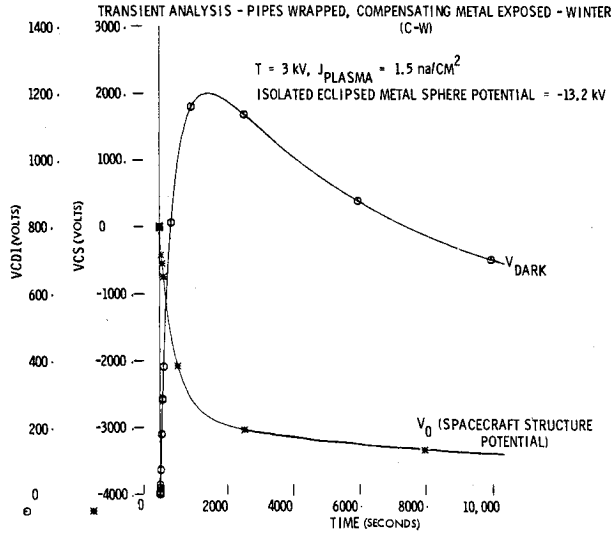

Fig. 11 Transient analysis Flights 5 and 6 configuration (winter).

Figures 10 and 11 show the types of time dependent results obtained for a 3 kev step-function substorm during the winter solstice. The nonlinear I-V characteristics of 2-mil kapton have been included in these two cases. Figure 10 is for the Flights 3 and 4 spacecraft now in orbit, and Fig. 11 applies to Flights 5 and 6, which are to be launched in 1975. Figure 9 shows a V_0 peak of -2.1 kv at $t = 1500$ sec for Flights 3 and 4, whereas V_0 only varies unidirectionally toward -3.5 kv with a time constant in the order of 1500 sec on Flights 5 and 6. The second curve in each of the figures, V_{dark}, is the potential difference, stress, between V_0 and V_1, the nonilluminated surface. V_{dark} on Flights 3 and 4 increases monotonically toward 2.6 kv, whereas it peaks at 1.2 kv on Flights 5 and 6, and stabilizes at 0.5 kv in the steady state.

Figures 12 and 13 show the variation of steady-state stress, (V_{dark}), with substorm temperature during the winter solstice. Curves A refer to the Flights 3 and 4 configuration and curves C refer to the Flights 5 and 6 configuration. Curves B represent an intermediate case between A and C. The abcissa in these two figures are marked in electron temperatures (kv) and also in terms of potential attained by an eclipsed metal sphere in the Maxwellian plasma at temperature T_e. At a temperature of 5 kev, for instance, the sphere potential would be -23 kv. Figure 12 shows the stresses obtained without the nonlinear I-V characteristics, and Fig. 12 the result with the nonlinear effects included. In both cases Flights 5 and 6 show

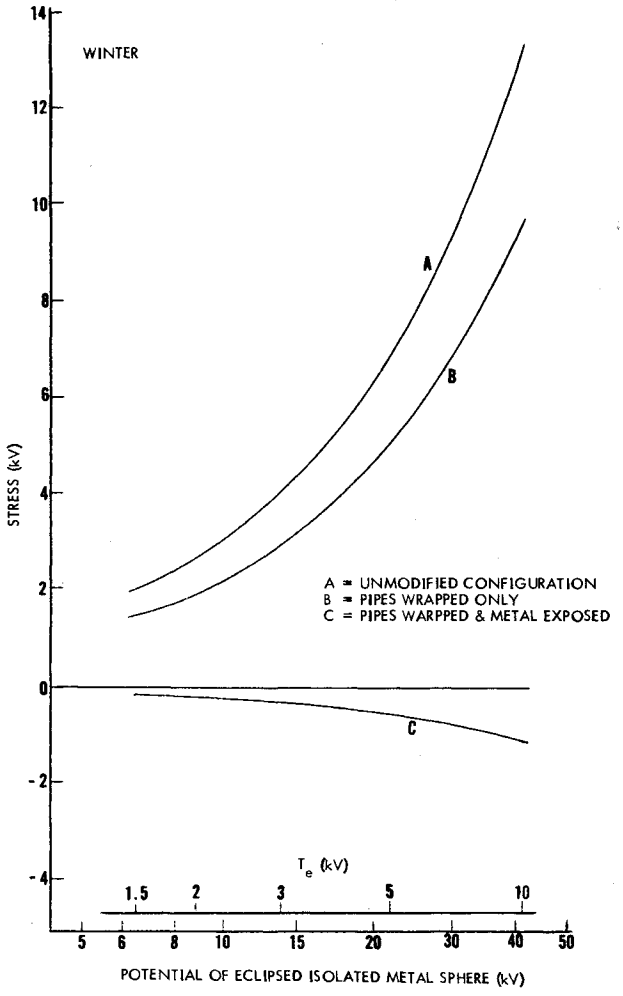

Fig. 12 Stress in forward closure dielectric surfaces nonlinear resistances excluded.

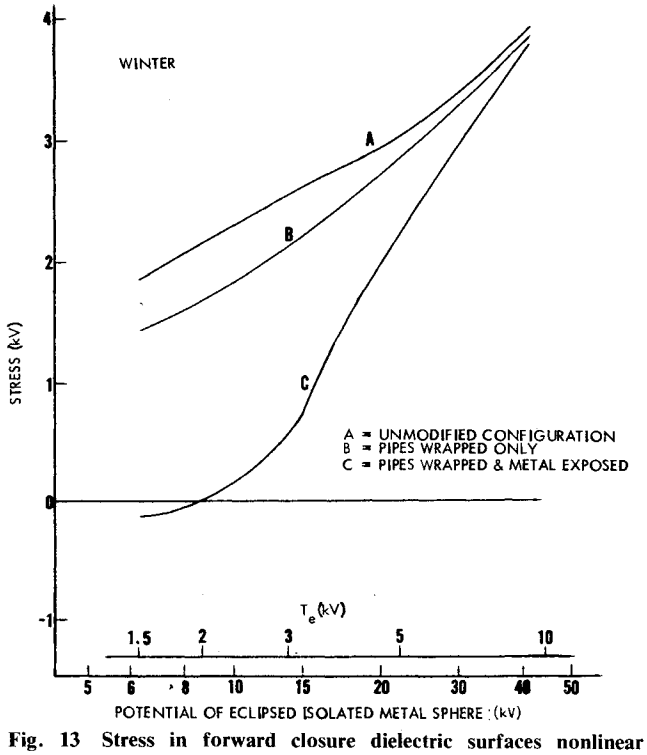

Fig. 13 Stress in forward closure dielectric surfaces nonlinear resistances included.

reduced stress over Flights 3 and 4. With the nonlinear resistance included, the effectiveness of the modifications is reduced as compared to the case in which nonlinearity is not taken into account. On the other hand, the overall levels of stress, the potential differences, are lower if nonlinear effects are included, because the leakage resistances become smaller with increasing voltage.

Discussion and Conclusions

The comparison in Table 4 of calculated stress levels in the Flights 5 and 6 configuration to those for the Flights 3 and 4 configuration show in general a decrease in stress. Special attention was focussed on $V_1 - V_0$, the stress between the forward closure surface and spacecraft ground, because all of the "T" and "C" type anomalies are related to the equipment on the despun platform right below. The increase in stress, $V_3 - V_0$, from 0 to 4.7 kv in the area below the spinning platform in going from Mod 0 to Mod 2 in the winter is not serious, since an even greater stress (-5.5 kv), exists in Mod 0 in the equinox season. The aperture stress due to sunlight, $V_4 - V_0$, of 5.5 kv in the equinox for Mod 0 (Flights 3 and 4) is consistent in its location with the "S" type of anomalies observed during the fall equinox.

The analytic model described here is necessarily a gross simplification of the actual case. For example, the current sources to a given capacitor (surface) are assumed to be independent of the potential of the other surfaces of the spacecraft. The formulation of the functional dependence of current on potential used was derived for equipotential spheres in an isotropic flux of particles with a Maxwell-Boltzmann energy distribution. Other areas of complexity ignored here are the presence of a plasma sheath due to secondary emission and photoemission,[13] and the external coupling via the plasma sheath between circuit elements (surface areas) which are at different potentials. Secondary and photoemission of electrons from a surface would be affected by the existence of a potential minimum of a few volts outside of the surface because the emission energies are in this range. Evaluations for ambient particles with energies in the kev range, however, would still be valid.

The validity of the results obtained from the calculations with the spacecraft charging model is obviously no better than the parameters put into it. Another limitation on validity, however, is that the results should be consistent with available data, such as the seasonal timing and the location on the spacecraft of the observed events on Flights 3 and 4. The analysis shows the dependence of the results on the various parameters involved. For the present purposes many of these parameters were taken from the available literature. The values of photoemission and secondary emission used are consistent with available data. Widely divergent values from those used, for instance, would have resulted in stress values which had a different seasonal dependence or no seasonal dependence at all. Much more directly applicable data are needed in the areas of materials parameters, such as photoemission and secondary emission as well as in the definition of the environmental plasma parameters.

The model serves a function of predicting the problem areas in spacecraft design which may exist as a result of differential charging. Counter-measures should be taken in the areas of desensitizing circuits to withstand the resulting arc discharge environment. Investigations should be instituted into the selection of materials for reducing electrostatic stress in terms of conductivity, secondary emission, and photoemission properties.

Finally, more diagnostic housekeeping type of on-board monitoring of spacecraft differential charging/arc discharging should be incorporated into every spacecraft put into the synchronous orbit environment. The rationale for this would be similar to that for monitoring temperatures, currents, and voltages. These are routinely incorporated on every spacecraft to check on its state of health and as a diagnostic in case of anomalous behavior.

Scientific spacecraft to define the synchronous orbit environment and to determine material properties in the environment are required to provide data essential for the proper design of operational spacecraft. Refinements of the present model would be useful in evaluating this type of information as it might affect any given spacecraft configuration.

References

[1]DeForest, S.E., Spacecraft Charging at Synchronous Orbit," *Journal of Geophysical Research,* Vol. 77, Feb. 1972, pp. 651-659.

[2]DeForest, S.E., "Electrostatic Potentials Developed by ATS-5," *Photon and Particle Interaction with Surfaces in Space,* R.J.L. Grard, ed., D. Reidel Pub. Co., Dordrecht-Holland, 1973, pp. 263-276.

[3]Shaw, R.R., "Electrical Discharges Caused by Satellite Charging at Synchronous Altitudes," Report No. 5078-01, July 1974, Aerojet Electrosystems Co., Azusa, Calif.

[4]Cauffman, D.P. and Shaw, R.R., "Transient Currents Generated by Electrical Discharges," *Space Science Instrumentation,* Vol. 1, Feb. 1975, pp. 125-137.

[5]Rosen, A., et al., "Final Report RGA Analysis: Findings Regarding Correlation of Satellite Anomalies with Magnetospheric Substorms, and Laboratory Test Results," 09670-7020-R0-00, Aug. 1, 1972, TRW Systems Group, Redondo Beach, Calif.

[6]"Final Report TDAL Gain State Analysis," 09670-7040-RU-00, Oct. 18, 1973, TRW Systems Group, Redondo Beach, Calif.

[7]DeForest, S. E., McPherron, R. L., and Rostoker, G., "The Possibility of an Environmental Origin for TDAL Anomalies of the DSCS-II Satellites," Appendix A.2-2D, *Final Technical Report Program 77 Anomaly Investigation for Satellites 9433 and 9434,* 09670 RFP 050-01, March 22, 1974, TRW Systems Group, Redondo Beach, Calif.

[8]Inouye, G. T., Vogl, J. L., Sellen Jr., J. M., DeForest, S. E., and Rosen, A., "Final Report Spacecraft Charging Analysis: Study and Analysis of the DSCS-11 Spacecraft Orbital Charging Phenomena," Aug. 16, 1974, TRW Systems Group, Redondo Beach, Calif.

[9]Knott, K., "Equilibrium Potential of a Magnetospheric Satellite in an Eclipse Situation," *Planetary & Space Sciences,* Vol. 20, 1972, pp. 1137-1146.

[10]Grard, R.J.L., Knott, L., and Pedersen, A., "Influence of Photoelectron Emission on Electric Field Measurements in the Magnetosphere and Solar Wind," Photon and Particle Interaction with Surfaces in Space, R.J.L. Grard, ed., D. Reidel Pub. Co., Dordrecht-Holland, 1973, pp. 163-189.

[11]Fredricks, R.W. and Scarf, F.L., "Observations of Spacecraft Charging Effects in Energetic Plasma Regions," *Photon & Particle Interactions with Surfaces in Space,* R.J.L. Grard, ed., D. Reidel Pub. Co., Dordrecht-Holland, 1973, pp. 277-308.

[12]Hoffmaster, D. and Sellen, J.M., Jr., "Electron Swarm Tunnel Measurements of Kapton Bulk Resistivity at High Electric Stress Levels," 4351.3.74-39, Sept. 5, 1974, TRW Systems Group, Redondo Beach, Calif.

[13]Whipple, E.C., Jr., "Theory of the Spherically Symetric Photosheath; A Thick Sheath Approximation," accepted for publication in *Journal of Geophysical Research.*